


Higgs decays to $Z\gamma$ and $\gamma\gamma$ in the flavor-gauged two Higgs doublet model*

Feng-Zhi Chen (陈丰之)[#] Qiaoyi Wen (温侨毅)[#] Fanrong Xu (徐繁荣)[†]

Department of Physics, College of Physics & Optoelectronic Engineering, Jinan University, Guangzhou 510632, China

Abstract: This study examines the $h \rightarrow Z\gamma$ and $h \rightarrow \gamma\gamma$ decays in the flavor-gauged two Higgs doublet model (FG2HDM), which augments the Standard Model (SM) with an additional scalar doublet, a singlet, and a $U(1)'$ flavor gauge symmetry. Beyond the SM spectrum, FG2HDM predicts five additional physical scalars and a new neutral gauge boson, Z' . We demonstrate that while both decay channels are sensitive to charged Higgs loops, $h \rightarrow Z\gamma$ is uniquely modified by fermion-antifermion- Z ($f\bar{f}Z$) vertex corrections. These vertex corrections further impact top-quark observables and the flavor-changing neutral current (FCNC) process $b \rightarrow s\ell^+\ell^-$. Our analysis identifies a viable parameter space ($m_{H^\pm} > 200$ GeV and $\lambda_{hH^+H^-} < 0$) consistent with current 1σ experimental limits, where the signal strength $\mu_{\gamma\gamma}$ remains the primary constraint on scalar sector parameters. Regarding the $f\bar{f}Z$ couplings, we delineate the allowed regions in the Q_{tL} - Q_{tR} plane by evaluating the leading top-quark contributions, revealing that $b \rightarrow s\ell^+\ell^-$ imposes the most stringent bounds. Finally, we highlight that the 14% projected precision for $\mu_{Z\gamma}$ at the High-Luminosity LHC (HL-LHC) will significantly enhance sensitivity to the FG2HDM.

Keywords: 2HDM, Higgs decay, B anomalies

DOI: 10.1088/1674-1137/ae4a07 **CSTR:** 32044.14.ChinesePhysicsC.50063102

I. INTRODUCTION

The discovery of the Higgs boson at the Large Hadron Collider (LHC) by the ATLAS and CMS collaborations in 2012 marked a significant triumph for the SM [1–3]. Despite the significant progress made in particle physics, several fundamental questions remain unanswered, such as the matter-antimatter asymmetry in the universe, the origin of neutrino mass, and the nature of dark matter. These unsolved mysteries underscore the limitations of the SM. Since then, the quest for new physics (NP) beyond the SM (BSM) has been one of the central endeavors in elementary particle physics.

One attractive extension to the SM, which involves adding an additional Higgs doublet, was first proposed by T. D. Lee to introduce the spontaneous CP violation [4] and is now dubbed the two Higgs doublet model (2HDM). However, a major drawback of the generic 2HDM is that it typically introduces the tree-level FCNCs in Yukawa interactions that are unexpected in a model construction. FCNC generation is suppressed by raising

various modified 2HDMs to control the two Yukawa interactions. This includes imposing different Z_2 charges for the two scalars [5, 6], aligning the two Yukawa matrices [7–9], or making the two Yukawa interactions proportional to the off-diagonal elements of the Cabibbo–Kobayashi–Maskawa (CKM) matrix [10, 11]. The last one is usually called the Branco–Grimus–Lavoura (BGL) model, named after the authors of this model [12]. A flavor gauged version of the BGL model, *i.e.*, FG2HDM, was first proposed in Ref. [13] and was further developed in Refs. [14–16]. FG2HDM extends the original 2HDM by incorporating a scalar singlet field and an additional $U(1)'$ flavor gauge symmetry. Compared with the SM particle spectrum, FG2HDM features five additional physical scalars and one neutral gauge boson Z' .

Recently, the ATLAS and CMS collaborations reported initial evidence for the $h \rightarrow Z\gamma$ decay. The observed signal strength¹⁾ $\mu_{Z\gamma}$ was measured at the 68% confidence level (CL) to be $2.0_{-0.9}^{+1.0}$ by ATLAS [17], 2.4 ± 0.9 by CMS [18], and 2.2 ± 0.7 in their combined analysis [19].

Received 27 November 2025; Accepted 24 February 2026; Accepted manuscript online 25 February 2026

* Supported by NSFC (12475095, U1932104), the Fundamental Research Funds for the Central Universities (11623330) and the 2024 Guangzhou Basic and Applied Basic Research Scheme Project for Maiden Voyage (2024A04J4190)

[†] E-mail: fanrongxu@jnu.edu.cn (Corresponding author)

[#] These authors contributed equally as the first authors

1) The signal strength μ_X (where X is any Higgs decay product) is defined as the product of the cross section and the branch fraction ($\sigma(pp \rightarrow h)\mathcal{B}(h \rightarrow X)$) relative to the SM prediction. The cross section aligns well with the SM prediction, so we assumed that the NP merely affect the branching fractions.



Content from this work may be used under the terms of the Creative Commons Attribution 3.0 licence. Any further distribution of this work must maintain attribution to the author(s) and the title of the work, journal citation and DOI. Article funded by SCOAP³ and published under licence by Chinese Physical Society and the Institute of High Energy Physics of the Chinese Academy of Sciences and the Institute of Modern Physics of the Chinese Academy of Sciences and IOP Publishing Ltd

Such a signal strength deviates from the SM prediction $\mu_{Z\gamma}^{\text{SM}} = 1$ by 1.9σ , motivating many possible explanations from two distinct perspectives. First, as $h \rightarrow Z\gamma$ is a loop-induced process, higher-order corrections to the leading-order (LO) amplitudes from one-loop amplitudes are crucial.¹⁾ These include two-loop QCD corrections [21–24], providing a 0.3% increase, and two-loop electroweak corrections [25, 26], yielding a 7% enhancement. Clearly, these next-to-leading-order (NLO) corrections alone cannot account for the 1.9σ excess. Alternatively, the deviation may stem from BSM contributions, a possibility extensively explored in the literature (e.g., [27–44]). However, integrating the most recent ATLAS measurement ($\mu_{Z\gamma} = 0.9_{-0.6}^{+0.7}$) [45] with previous results yields a revised signal strength of $\mu_{Z\gamma} = 1.3_{-0.5}^{+0.6}$, bringing the observation into agreement with SM expectations. While this reduces the immediate tension, analysing $h \rightarrow Z\gamma$ within specific BSM frameworks still requires a simultaneous consideration of the $h \rightarrow \gamma\gamma$ channel. This is due to the inherent correlation between the two, as both are mediated by the same charged loop-particles [46, 47]. Given that the current experimental value $\mu_{\gamma\gamma} = 1.10 \pm 0.06$ [48], highly accords with the SM, it imposes stringent constraints on the FG2HDM parameter space, effectively narrowing the regions permitted by the $\mu_{Z\gamma}$ data.

Building on our previous work [49], where specific Yukawa matrix textures in FG2HDM were proposed to explain the long-standing B anomalies, the present study investigates whether the model's parameter space remains viable under the current experimental constraints on $\mu_{Z\gamma}$ and $\mu_{\gamma\gamma}$. While the $h \rightarrow Z\gamma$ and $h \rightarrow \gamma\gamma$ channels have been explored in other frameworks such as the complex 2HDM (C2HDM) [50] using earlier data [51, 52], the recent updates from ATLAS and CMS [17–19, 45] necessitate a more refined numerical and theoretical analysis. In FG2HDM, both decay modes receive loop-level contributions from charged Higgs bosons; furthermore, $h \rightarrow Z\gamma$ is modified by corrections to the $f\bar{f}Z$ vertex. Consequently, this work aims to identify the permitted FG2HDM parameter space for $\mu_{Z\gamma}$ and $\mu_{\gamma\gamma}$ while accounting for the constraints on the $f\bar{f}Z$ vertex from top-quark measurements and the $b \rightarrow s\ell^+\ell^-$ FCNC process.

The remainder of the paper is organized as follows: In Sec. II, we provide a brief overview of the key features of FG2HDM. In Sec. III, we calculate the one-loop amplitudes for the $h \rightarrow Z\gamma$ and $h \rightarrow \gamma\gamma$ decays in the unitary gauge. The numerical analysis and subsequent discussions are detailed in Sec. IV. Our conclusions are presented in Sec. V. For convenience, the relevant Lagrangian and the corresponding Feynman rules are prepared in Ap-

pendix A. In addition, the explicit expressions for the scalar functions obtained from one-loop calculations are listed in Appendix B, along with the kinematics for Higgs decays in Appendix C.

II. THE MODEL

FG2HDM is a specific 2HDM comprising two $SU(2)_L$ scalar doublets, Φ_1 and Φ_2 , and a scalar singlet S , and endowed with an additional $U(1)'$ flavor gauge symmetry. Here, the $U(1)'$ charges, denoted as X_i ($i = L_L, \dots, S$), are assigned to ensure $U(1)'$ gauge invariance. The detailed relationships among these $U(1)'$ charges for various fields are elaborated in Appendix A of Ref. [49]. In the presence of the new $U(1)'$ gauge symmetry, the gauge anomaly constraints should be considered further. Note that various anomaly-free FG2HDMs have been surveyed and studied in Refs. [14–16].

For convenience, we collect the quantum representations for various fields in FG2HDM under the $SU(2)_L \times U(1)_Y \times U(1)'$ symmetries in Table 1. With these assignments, the total Lagrangian of FG2HDM can be expressed as [49]

$$\mathcal{L} = \mathcal{L}_S + \mathcal{L}_G + \mathcal{L}_F, \quad (1)$$

where subscripts S , G , and F denote respectively for the scalar, gauge, and fermion components of the total Lagrangian.²⁾

$$\begin{aligned} \mathcal{L}_S = & D^\mu \Phi_1^\dagger D_\mu \Phi_1 + D^\mu \Phi_2^\dagger D_\mu \Phi_2 \\ & + D^\mu S^* D_\mu S - V(\Phi_1, \Phi_2, S), \end{aligned} \quad (2)$$

$$\mathcal{L}_G = -\frac{1}{4} W_{\mu\nu}^a W^{a\mu\nu} - \frac{1}{4} B_{\mu\nu} B^{\mu\nu} - \frac{1}{4} \hat{Z}'_{\mu\nu} \hat{Z}'^{\mu\nu}, \quad (3)$$

$$\begin{aligned} \mathcal{L}_F = & \bar{Q}_L i D_\mu \gamma^\mu Q_L + \bar{L}_L i D_\mu \gamma^\mu L_L + \bar{u}_R i D_\mu \gamma^\mu u_R \\ & + \bar{d}_R i D_\mu \gamma^\mu d_R + \bar{e}_R i D_\mu \gamma^\mu e_R \\ & - \left[\bar{Q}_L (Y_1^d \Phi_1 + Y_2^d \Phi_2) d_R + \bar{Q}_L (Y_1^u \tilde{\Phi}_1 + Y_2^u \tilde{\Phi}_2) u_R \right. \\ & \left. + \bar{L}_L (Y_1^\ell \Phi_1 + Y_2^\ell \Phi_2) e_R + \text{h.c.} \right]. \end{aligned} \quad (4)$$

where $L_L = (\nu_L, e_L)^T$ and $Q_L = (u_L, d_L)^T$ represent the left-handed lepton and quark $SU(2)_L$ doublets, respectively, and e_R , u_R , and d_R denote the right-handed lepton, up-

1) Refer to Ref. [20] for an estimated magnitude of leading non-perturbative QCD corrections (10^{-5}).

2) In principle, Eq. (3) could include a gauge-symmetry-allowed kinetic mixing term, $-\frac{\sin\epsilon}{2} B_{\mu\nu} \hat{Z}'^{\mu\nu}$, which would primarily result in a redefinition of the $U(1)'$ charges. However, since its effect is to shift the constraints from the original $U(1)'$ charges to these redefined ones without altering the numerical results or physical predictions of the model, we can safely neglect this term for simplicity.

Table 1. Quantum numbers of different fields under the $SU(3)_C \times SU(2)_L \times U(1)_Y \times U(1)'$ symmetries.

Fields	L_L	e_R	Q_L	u_R	d_R	Φ_1	Φ_2	S
$SU(3)_C$	1	1	3	3	3	1	1	1
$SU(2)_L$	2	1	2	1	1	2	2	1
$U(1)_Y$	$-\frac{1}{2}$	-1	$\frac{1}{6}$	$\frac{2}{3}$	$-\frac{1}{3}$	$\frac{1}{2}$	$\frac{1}{2}$	0
$U(1)'$	X_{L_L}	X_{e_R}	X_{Q_L}	X_{u_R}	X_{d_R}	X_{Φ_1}	X_{Φ_2}	X_S

type quark, and down-type quark $SU(2)_L$ singlets, respectively. The physical significance of each component is elaborated subsequently.

The scalar potential in Eq. (2) is given by [49]

$$\begin{aligned}
V(\Phi_1, \Phi_2, S) = & m_{11}^2 \Phi_1^\dagger \Phi_1 + m_{22}^2 \Phi_2^\dagger \Phi_2 \\
& + \frac{\lambda_1}{2} (\Phi_1^\dagger \Phi_1)^2 + \frac{\lambda_2}{2} (\Phi_2^\dagger \Phi_2)^2 \\
& + \lambda_3 (\Phi_1^\dagger \Phi_1) (\Phi_2^\dagger \Phi_2) + \lambda_4 (\Phi_1^\dagger \Phi_2) (\Phi_2^\dagger \Phi_1) \\
& + m_S^2 |S|^2 + \lambda_S |S|^4 + \kappa_1 |\Phi_1|^2 |S|^2 + \kappa_2 |\Phi_2|^2 |S|^2 \\
& + \kappa_3 (\Phi_1^\dagger \Phi_2 S^2 + \Phi_2^\dagger \Phi_1 (S^*)^2),
\end{aligned} \quad (5)$$

where $m_{11,22,S}$, $\lambda_{1,2,3,4,S}$, and $\kappa_{1,2,3}$ denote the coupling constants of various interaction terms. The two doublets and the singlet in the flavor basis are parametrized as

$$\begin{aligned}
\Phi_1 = & \begin{pmatrix} \phi_1^+ \\ \frac{1}{\sqrt{2}}(\rho_1 + i\eta_1 + \nu_1) \end{pmatrix}, \quad \Phi_2 = \begin{pmatrix} \phi_2^+ \\ \frac{1}{\sqrt{2}}(\rho_2 + i\eta_2 + \nu_2) \end{pmatrix}, \\
S = & \frac{1}{\sqrt{2}}(s_0 + i\chi_0 + \nu_S),
\end{aligned} \quad (6)$$

where the vacuum expectation values (VEVs) ν_1 and ν_2 combine to form the SM Higgs VEV $v = 1/(\sqrt{2}G_F)^{1/2} = \sqrt{\nu_1^2 + \nu_2^2} \simeq 246$ GeV, with G_F being the Fermi constant. The singlet VEV ν_S is introduced to spontaneously break the $U(1)'$ symmetry. Rotating to the mass basis yields

$$\begin{aligned}
\begin{pmatrix} G^\pm \\ H^\pm \end{pmatrix} = & U_1 \begin{pmatrix} \phi_1^\pm \\ \phi_2^\pm \end{pmatrix}, \quad \begin{pmatrix} G^0 \\ G'^0 \\ H_A \end{pmatrix} = U_2 \begin{pmatrix} \eta_1 \\ \eta_2 \\ \chi_0 \end{pmatrix}, \\
\begin{pmatrix} H \\ h \\ H_S \end{pmatrix} = & U_3 \begin{pmatrix} \rho_1 \\ \rho_2 \\ s_0 \end{pmatrix},
\end{aligned} \quad (7)$$

where U_1 , U_2 , and U_3 are the rotation matrices defined as

$$\begin{aligned}
U_1 \equiv & \begin{pmatrix} \cos\beta & \sin\beta \\ -\sin\beta & \cos\beta \end{pmatrix}, \quad U_2 \equiv \begin{pmatrix} 1 & 0 \\ 0 & U_\gamma \end{pmatrix} \begin{pmatrix} U_1 & 0 \\ 0 & 1 \end{pmatrix}, \\
U_3 \equiv & \begin{pmatrix} -\cos\alpha & -\sin\alpha & 0 \\ \sin\alpha & -\cos\alpha & 0 \\ 0 & 0 & 1 \end{pmatrix}.
\end{aligned} \quad (8)$$

Here, α and β are the rotation angles, and U_γ and $\tan 2\alpha$ are given by

$$\begin{aligned}
U_\gamma = & \begin{pmatrix} \frac{2\nu_1\nu_2}{\sqrt{4\nu_1^2\nu_2^2 + \nu^2\nu_S^2}} & \frac{-\nu\nu_S}{\sqrt{4\nu_1^2\nu_2^2 + \nu^2\nu_S^2}} \\ \frac{\nu\nu_S}{\sqrt{4\nu_1^2\nu_2^2 + \nu^2\nu_S^2}} & \frac{2\nu_1\nu_2}{\sqrt{4\nu_1^2\nu_2^2 + \nu^2\nu_S^2}} \end{pmatrix}, \\
\tan 2\alpha = & \frac{2l}{m-n},
\end{aligned} \quad (9)$$

where

$$\begin{aligned}
m = & \lambda_1\nu_1^2 - \frac{1}{2}\kappa_3\frac{\nu_2}{\nu_1}\nu_S^2, \quad n = \lambda_2\nu_2^2 - \frac{1}{2}\kappa_3\frac{\nu_1}{\nu_2}\nu_S^2, \\
l = & \lambda_{34}\nu_1\nu_2 + \frac{1}{2}\kappa_3\nu_S^2.
\end{aligned} \quad (10)$$

After spontaneous symmetry breaking, the four undesired Goldstone bosons G^\pm , G^0 , and G'^0 in Eq. (7) are "eaten" to give masses to the W^\pm , Z , and Z' gauge bosons, respectively. This leaves us with six physical scalars: two charged Higgs H^\pm ; three neutral scalars H , h , and H_S ; and one neutral pseudoscalar H_A . Their masses are separately given by

$$\begin{aligned}
m_{h,H}^2 = & \frac{1}{2} \left[(m+n) \mp \sqrt{(m-n)^2 + 4l^2} \right], \\
m_{H_S}^2 = & 2\lambda_S\nu_S^2, \\
m_{H_A}^2 = & -\frac{1}{2}\kappa_3 \left(4\nu_1\nu_2 + \frac{\nu^2\nu_S^2}{\nu_1\nu_2} \right), \\
m_{H^\pm}^2 = & -\frac{1}{2} \left(\lambda_4\nu^2 + \frac{\kappa_3\nu^2\nu_S^2}{\nu_1\nu_2} \right).
\end{aligned} \quad (11)$$

Among the four neutral particles, h , H , and H_S are CP-even, while H_A is CP-odd. Notably, the scalar h is identified as the Higgs boson discovered at the LHC in 2012 [1–3].

In Eqs. (2) and (4), the covariant derivatives for the $SU(2)_L$ doublets and singlets are defined, respectively, as follows:

$$D_\mu = \partial_\mu - ig_1 Y_i B_\mu - ig' X_i \hat{Z}'_\mu - ig_2 \frac{\tau^a}{2} W_\mu^a, \quad (12)$$

$$D_\mu = \partial_\mu - ig_1 Y_i B_\mu - ig' X_i \hat{Z}'_\mu, \quad (13)$$

where τ^a ($a = 1, 2, 3$) is the Pauli matrix, and B_μ , \hat{Z}'_μ , and W_μ^a are the $U(1)_Y$, $U(1)'$ and $SU(2)_L$ gauge bosons, respectively. Here, g_1 , g' , and g_2 are the corresponding coupling constants, and Y_i and X_i denote the hypercharge and $U(1)'$ charge of the fields, respectively. After spontaneous symmetry breaking, the gauge bosons acquire their masses. The transformation from the flavor to mass basis is achieved through the mixing matrix, as follows:

$$\begin{pmatrix} A \\ Z \\ Z' \end{pmatrix} = U \begin{pmatrix} B \\ W^3 \\ \hat{Z}' \end{pmatrix}, \quad U = \begin{pmatrix} \cos\theta_W & \sin\theta_W & 0 \\ -\sin\theta_W \cos\theta'_2 & \cos\theta_W \cos\theta'_2 & \sin\theta'_2 \\ \sin\theta_W \sin\theta'_2 & -\cos\theta_W \sin\theta'_2 & \cos\theta'_2 \end{pmatrix}, \quad (14)$$

where θ_W is the Weinberg angle, and θ'_2 the mixing angle between Z and Z' . In the limit where θ'_2 approaches zero, the mixing restores to the case in the SM. This arrangement introduces the tree-level FCNCs in the down-type quark sector, which can account for the anomalies observed in B physics [49]. In addition, it generates off-diagonal interactions, with the Higgs and Z boson coupling to the charged Higgs and W boson, as well as new corrections to the $f\bar{f}Z$ couplings, thereby causing FG2HDM to contribute more to $h \rightarrow Z\gamma$ than $h \rightarrow \gamma\gamma$.

The interactions between fermions and gauge bosons are derived from the covariant derivative terms in the first line of Eq. (4). These terms encapsulate how fermions couple to the gauge bosons associated with the symmetries of the model. Meanwhile, the remaining terms in Eq. (4) depict the Yukawa interactions between fermions and the scalar doublets.¹⁾ After spontaneous symmetry breaking, the scalar fields acquire VEVs, which give masses to the fermions.

Armed with the Lagrangian of FG2HDM, we can derive the relevant Feynman rules. In this context, we concentrate solely on the crucial terms indispensable for computing the one-loop amplitudes of the $h \rightarrow Z\gamma$ and $h \rightarrow \gamma\gamma$ decays. These vital terms, together with their corresponding Feynman rules, are cataloged in Appendix A.

III. ONE-LOOP AMPLITUDES

Following a general Lorentz decomposition while enforcing photon gauge invariance, as detailed in Ref. [23],

we can express the amplitudes for the processes $h(p) \rightarrow Z(p_1)\gamma(p_2)$ and $h(p) \rightarrow \gamma(p_1)\gamma(p_2)$ in the following form:

$$\mathcal{M}_X = (p_2^\mu p_1^\nu - p_1 \cdot p_2 g^{\mu\nu}) T_X \epsilon_\mu^*(p_1) \epsilon_\nu^*(p_2), \quad X = Z\gamma, \gamma\gamma, \quad (15)$$

where $\epsilon_{\mu(\nu)}$ represents the polarization vector of the Z boson or photon, and T_X denotes the one-loop functions to be determined. In the presence of NP, the function T_X can be written as $T_X = T_X^{\text{SM}} + T_X^{\text{NP}}$, and the signal strength μ_X is defined as

$$\mu_X = \left| 1 + \frac{T_X^{\text{NP}}}{T_X^{\text{SM}}} \right|^2. \quad (16)$$

Utilizing the Feynman rules for vertices and propagators outlined in Fig A1 of Appendix A, we can determine the one-loop Feynman diagrams for the decays $h \rightarrow Z\gamma$ and $h \rightarrow \gamma\gamma$, as depicted in Figs. 1 and 2. We have omitted the diagrams containing off-diagonal fermions in the loops, given the strong suppression of the FCNCs. Upon examining the Feynman diagrams for $h \rightarrow Z\gamma$ and $h \rightarrow \gamma\gamma$, an additional class of diagrams with off-diagonal couplings to the Higgs and Z boson is observed for $h \rightarrow Z\gamma$ (*i.e.*, the last row of Fig. 1),²⁾ which suggests a greater contribution of the FG2HDM to $h \rightarrow Z\gamma$ relative to $h \rightarrow \gamma\gamma$. Furthermore, the novel corrections to the $f\bar{f}Z$ couplings offer an alternative pathway to enhance the contribution to $h \rightarrow Z\gamma$, as previously discussed in Sec. I. The one-loop functions T_X can then be extracted by

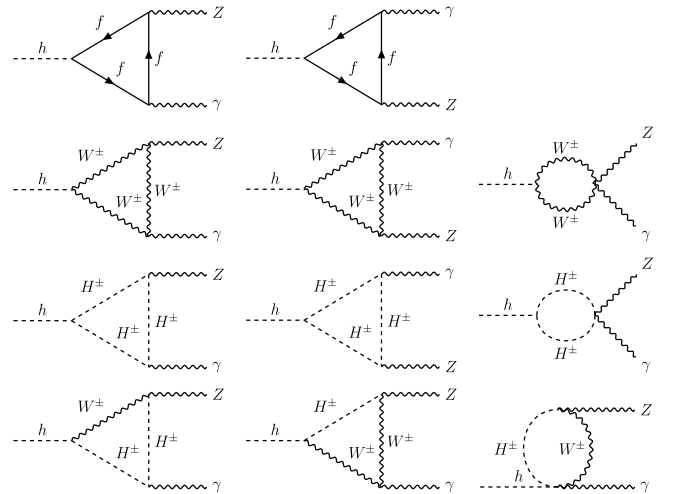


Fig. 1. One-loop Feynman diagrams for $h \rightarrow Z\gamma$.

1) Note that in these Yukawa interactions, the right-handed charged leptons and down-type quarks couple directly to Φ_i . In contrast, the right-handed up-type quarks couple to the charge-conjugate fields, $\bar{\Phi}_i \equiv i\tau^2 \Phi_i^*$.

2) Note that such diagrams have never appeared in other Higgs models, see, *e.g.*, Refs. [46,53].

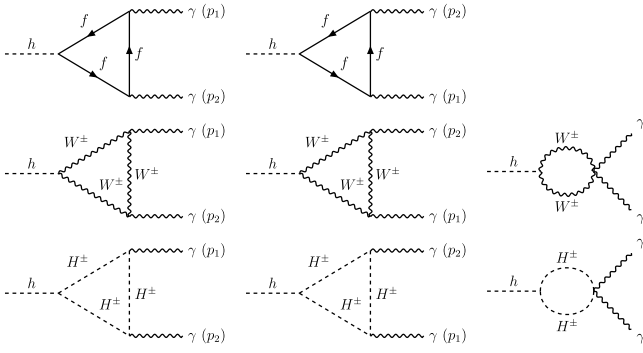


Fig. 2. One-loop Feynman diagrams for $h \rightarrow \gamma\gamma$.

matching onto the calculations of the one-loop Feynman diagrams. In this study, we calculate these diagrams using *Package-X* [54], as follows:

A. $h \rightarrow Z\gamma$

The one-loop Feynman diagrams that contribute to

the $h \rightarrow Z\gamma$ process are depicted in Fig. 1. We have intentionally omitted the external legs self-energy diagrams for this decay mode because they lack the Lorentz structure specified in Eq. (15), and the divergences present in the calculations of the Feynman diagrams in each row of Fig. 1 are found to cancel each other out (a pattern that also applies to $h \rightarrow \gamma\gamma$). These diagrams are categorized into four distinct classes (one row, one class), each corresponding to a type of particle involved in the internal lines. Consequently, the total one-loop function $T_{Z\gamma}$ is decomposed into the following four distinct components:

$$T_{Z\gamma} = T_{Z\gamma}^f + T_{Z\gamma}^W + T_{Z\gamma}^H + T_{Z\gamma}^{WH}, \quad (17)$$

corresponding to the contributions from fermions, W boson, charged Higgs, and mixed W boson and charged Higgs loops, respectively. Specifically,

$$T_{Z\gamma}^f = \sum_f \frac{eg_2 Q_f N_C m_f}{16\pi^2 m_W (m_h^2 - m_Z^2)^2} \left[\frac{g_2}{c_W} (I_f^3 - 2Q_f s_W^2) \cos\theta'_2 + g' (Q_{fL} + Q_{fR}) \sin\theta'_2 \right] [\sin(\alpha - \beta) M_f - \cos(\alpha - \beta) N_f] \\ \times \left\{ 4m_Z^2 [\Lambda(m_h^2; m_f, m_f) - \Lambda(m_Z^2; m_f, m_f)] + 2(m_h^2 - m_Z^2) \left[2 + (4m_f^2 - m_h^2 + m_Z^2) C_0(m_Z^2, 0, m_h^2, m_f^2, m_f^2, m_f^2) \right] \right\}, \quad (18)$$

$$T_{Z\gamma}^W = -\frac{eg_2^2 c_W \sin(\alpha - \beta) \cos\theta'_2}{16\pi^2 m_W^3 (m_h^2 - m_Z^2)^2} \left\{ [12m_W^4 - 2m_W^2 m_Z^2 + m_h^2 (2m_W^2 - m_Z^2)] [(m_h^2 - m_Z^2) + m_Z^2 (\Lambda(m_h^2; m_W, m_W) - \Lambda(m_Z^2; m_W, m_W))] \right. \\ \left. + 2m_W^2 (m_h^2 - m_Z^2) (12m_W^4 + 6m_W^2 m_Z^2 - 2m_Z^4 - 6m_h^2 m_W^2 + m_h^2 m_Z^2) C_0(m_Z^2, 0, m_h^2, m_W^2, m_W^2, m_W^2) \right\}, \quad (19)$$

$$T_{Z\gamma}^H = -\frac{4ev\lambda_{hH^+H^-}}{16\pi^2 (m_h^2 - m_Z^2)^2} \left[\left(\frac{g_2}{2} c_W - \frac{g_1}{2} s_W \right) \cos\theta'_2 + (\sin^2\beta Q_1 + \cos^2\beta Q_2) g' \sin\theta'_2 \right] \left\{ m_Z^2 [\Lambda(m_h^2; m_{H^\pm}, m_{H^\pm}) \right. \\ \left. - \Lambda(m_Z^2; m_{H^\pm}, m_{H^\pm}) \right] + (m_h^2 - m_Z^2) \left[1 + 2m_{H^\pm}^2 C_0(m_Z^2, 0, m_h^2, m_{H^\pm}^2, m_{H^\pm}^2, m_{H^\pm}^2) \right] \right\}, \quad (20)$$

$$T_{Z\gamma}^{WH} = \frac{eg_2 g' (Q_2 - Q_1) \cos(\alpha - \beta) \sin\beta \cos\beta \sin\theta'_2}{16\pi^2 m_W (m_h^2 - m_Z^2)} \left\{ 2(m_h^2 - m_{H^\pm}^2 + m_W^2) \left[\frac{m_Z^2}{m_h^2 - m_Z^2} (\Lambda(m_h^2; m_{H^\pm}, m_W) - \Lambda(m_Z^2; m_{H^\pm}, m_W)) \right. \right. \\ \left. \left. + \frac{m_{H^\pm}^2 - m_W^2}{2m_h^2} \log\left(\frac{m_{H^\pm}^2}{m_W^2}\right) + m_{H^\pm}^2 C_0(0, m_h^2, m_Z^2, m_{H^\pm}^2, m_{H^\pm}^2, m_W^2) + 1 \right] \right. \\ \left. - 2m_W^2 (m_h^2 + m_{H^\pm}^2 - m_W^2 - 2m_Z^2) C_0(0, m_h^2, m_Z^2, m_W^2, m_W^2, m_{H^\pm}^2) \right\}. \quad (21)$$

In Eq. (18), we have summed over the contributions from all the fermions, and the color factor N_C is 3 for quarks and 1 for leptons. The symbols Q_{Lf} , Q_{fR} , Q_1 , and Q_2 denote the $U(1)'$ charge of the left-handed fermions, right-handed fermions, Φ_1 , and Φ_2 , respectively. The defini-

tions of M_f , N_f (Eq. (18)) and the coupling, $\lambda_{hH^+H^-}$ (Eq. (20)), are provided in Appendix A. The analytical expressions for the scalar functions $\Lambda(m_a^2; m_b, m_c)$, $C_0(m_Z^2, 0, m_h^2, m_i^2, m_i^2, m_i^2)$, and $C_0(0, m_h^2, m_Z^2, m_i^2, m_i^2, m_i^2)$ in Eqs. (18)–(21) are listed in Appendix B. Note that similar expres-

sions for T_X can also be found in Ref. [50]. Notably, the novel contribution $T_{Z\gamma}^{WH}$, which arises from the $W^\pm H^\mp Z$ coupling and is uniquely present in FG2HDM, distinguishes it from other conventional 2HDMs.

B. $h \rightarrow \gamma\gamma$

The one-loop Feynman diagrams responsible for the $h \rightarrow \gamma\gamma$ process are illustrated in Fig. 2. In the depiction of the first and second diagrams in each row, distinct momenta p_1 and p_2 are assigned to differentiate the two identical photons in the final state. Paralleling the approach for $h \rightarrow Z\gamma$, the total one-loop function $T_{\gamma\gamma}$ is decomposed into three distinct parts:

$$T_{\gamma\gamma} = T_{\gamma\gamma}^f + T_{\gamma\gamma}^W + T_{\gamma\gamma}^H, \quad (22)$$

with each term explicitly given by

$$T_{\gamma\gamma}^f = \sum_f \frac{4e^2 g_2 N_C Q_f^2 m_f (\sin(\alpha - \beta) M_f - \cos(\alpha - \beta) N_f)}{16\pi^2 m_h^2 m_W} \times [2 + (4m_f^2 - m_h^2) C_0(0, 0, m_h^2, m_f^2, m_f^2, m_f^2)], \quad (23)$$

$$T_{\gamma\gamma}^W = \frac{-2e^2 g_2 \sin(\alpha - \beta)}{16\pi^2 m_h^2 m_W} [(m_h^2 + 6m_W^2 + (12m_h^4 - 6m_h^2 m_W^2) C_0(0, 0, m_h^2, m_W^2, m_W^2, m_W^2))], \quad (24)$$

$$T_{\gamma\gamma}^H = -\frac{4e^2 v \lambda_{hH^\pm H^\mp}}{16\pi^2 m_h^2} [1 + 2m_{H^\pm}^2 C_0(0, 0, m_h^2, m_{H^\pm}^2, m_{H^\pm}^2, m_{H^\pm}^2)]. \quad (25)$$

The analytical expressions for the scalar function $C_0(0, 0, m_h^2, m_i^2, m_i^2, m_i^2)$ in Eqs. (23)–(25) can also be found in Appendix B. Unlike in the $h \rightarrow Z\gamma$ process, no $T_{Z\gamma}^{WH}$ contribution occurs because the $W^\pm H^\mp \gamma$ interaction is forbidden in FG2HDM, as it is in other conventional 2HDMs and the SM.

IV. NUMERICAL ANALYSIS

In this section, we perform a numerical analysis to assess whether the parameter spaces of FG2HDM can simultaneously accommodate the current measured $\mu_{Z\gamma}$ and $\mu_{\gamma\gamma}$. For ease of reference, the input parameters used in the numerical analysis throughout this work are summarized in Table 2. It should be noted that the fine structure constant, $\alpha \equiv e^2/4\pi$, is scale dependent and is related to the electroweak gauge coupling g_2 via the relation $e = g_2 \sin\theta_W$. Additionally, we do not adopt the experimental value for Γ_h from the particle data group (PDG), which has a relatively large uncertainty ($\Gamma_h^{\text{PDG}} = 3.7_{-1.4}^{+1.9}$

Table 2. Relevant input parameters used in our numerical analysis.

$\sin^2 \theta_W = 0.23129(4)$	[48]	$m_W = 80.3692(133)$ GeV	[48]
$\alpha(0) = 1/137.036$	[48]	$m_Z = 91.1880(20)$ GeV	[48]
$\alpha(m_Z) = 1/127.944(14)$	[48]	$m_h = 125.20(11)$ GeV	[48]
$\Gamma_h = 4.07_{-3.9\%}^{+4.0\%}$ MeV	[55]	$m_t = 172.57(29)$ GeV	[48]
$G_F = 1.1663788 \times 10^{-5}$ GeV ⁻²	[48]	$m_\tau = 1.77693(9)$ GeV	[48]
$m_b = 4.183(7)$ GeV	[48]	$m_c = 1.2730(46)$ GeV	[48]
$m_s = 93.5(8)$ MeV	[48]	$m_\mu = 105.658$ MeV	[48]
$m_d = 4.70(7)$ MeV	[48]	$m_e = 0.511$ MeV	[48]
$m_u = 2.16(7)$ MeV	[48]		

MeV) [48], but rather, we cite the value with smaller uncertainty from Ref. [55]. Our strategy in this section initially involves calculating the SM LO contributions for the decays $h \rightarrow Z\gamma$ and $h \rightarrow \gamma\gamma$, whose numerical values provide valuable insights for NP model buildings. We then incorporate the corrections from FG2HDM in detail.

A. SM prediction

The expressions in Eqs. (18)–(21) and (23)–(25) revert to the SM formulas upon setting $\theta_2 \rightarrow 0$ and $\sin(\alpha - \beta) \rightarrow 1$. The numerical results for $T_{Z\gamma}$ (in the unit of GeV⁻¹) in the SM are then given by

$$\begin{aligned} T_{Z\gamma}^{W,\text{SM}} &= -5.866 \times 10^{-5}, & T_{Z\gamma}^{t,\text{SM}} &= 3.115 \times 10^{-6}, \\ T_{Z\gamma}^{b,\text{SM}} &= -6.685 \times 10^{-8} + 3.762 \times 10^{-8}i, \\ T_{Z\gamma}^{c,\text{SM}} &= -9.797 \times 10^{-9} + 3.864 \times 10^{-9}i, \\ T_{Z\gamma}^{\tau,\text{SM}} &= -1.731 \times 10^{-9} + 7.452 \times 10^{-10}i. \end{aligned} \quad (26)$$

Eq. (26) (and also Eq. (27)) clearly indicates that the dominant contributions arise from the W loops, and the secondary contributions come from the interference between the W and top quark loops. Contributions from the s , d , u , μ , and e loops are not presented here, as they are several orders of magnitude smaller than those we have displayed and therefore can be neglected safely. Likewise, the SM contributions to $T_{\gamma\gamma}$ (in the unit of GeV⁻¹) are

$$\begin{aligned} T_{\gamma\gamma}^{W,\text{SM}} &= -3.912 \times 10^{-5}, & T_{\gamma\gamma}^{t,\text{SM}} &= 8.619 \times 10^{-6}, \\ T_{\gamma\gamma}^{b,\text{SM}} &= -1.123 \times 10^{-7} + 1.485 \times 10^{-7}i, \\ T_{\gamma\gamma}^{c,\text{SM}} &= -9.103 \times 10^{-8} + 7.462 \times 10^{-8}i, \\ T_{\gamma\gamma}^{\tau,\text{SM}} &= -1.107 \times 10^{-7} + 1.011 \times 10^{-7}i. \end{aligned} \quad (27)$$

With the kinematics formula derived in Appendix C, the SM predictions for $h \rightarrow Z\gamma$ and $h \rightarrow \gamma\gamma$ are given separ-

ately by

$$\mathcal{B}(h \rightarrow Z\gamma)_{\text{SM}} = (1.536 \pm 0.018) \times 10^{-3}, \quad (28)$$

$$\mathcal{B}(h \rightarrow \gamma\gamma)_{\text{SM}} = (2.278 \pm 0.023) \times 10^{-3}, \quad (29)$$

which are respectively in good agreement with those given in Ref. [55]: $\mathcal{B}(h \rightarrow Z\gamma) = (1.5 \pm 0.1) \times 10^{-3}$ and $\mathcal{B}(h \rightarrow \gamma\gamma) = (2.27 \pm 0.07) \times 10^{-3}$.

B. Constraining FG2HDM parameters

The $h \rightarrow \gamma\gamma$ decay imposes stringent constraints on the FG2HDM parameters, as the SM prediction of $\mu_{\gamma\gamma}$ aligns well with its measurement. This implies that we should have $\sin(\alpha - \beta) \approx 1$ (or equivalently, $\cos(\alpha - \beta) \approx 0$) to ensure that $T_{\gamma\gamma}^f$ and $T_{\gamma\gamma}^W$ are close to their SM values, and the contribution from the charged Higgs loops should be minimal. Additionally, we should have $\cos\theta_2 \approx 1$ (or equivalently, $\sin\theta_2 \approx 0$) to ensure that the ZW^+W^- coupling does not deviate too much from its SM value.

With the aforementioned approximations, we can first determine the parameter regions for the charged Higgs interactions. They can be classified into two parts, *i.e.*, the pure charged Higgs diagrams and the W^\pm - H^\pm mixing diagrams. Note that the latter only contribute to $h \rightarrow Z\gamma$, which is actually negligible compared to the pure one. The analysis is as follows.

To estimate the magnitude of $T_{Z\gamma}^{WH}$ given in Eq. (21), we need to endow values for $\cos(\alpha - \beta)$ (or equivalently, $\sin(\alpha - \beta)$), g' , $Q_2 - Q_1$, $\cos\beta$ (or equivalently, $\sin\beta$), and $\sin\theta_2$. However, as we do not have the exact values for

these parameters, we can only make some rough but reasonable estimates. As discussed in the first paragraph of this subsection, to ensure that $T_{\gamma\gamma}^f$ and $T_{\gamma\gamma}^W$ do not deviate too much from their SM predictions, we should have $\cos(\alpha - \beta) \approx 0$ and $\sin\theta_2 \approx 0$. Note that the constraints from the B observables in our previous work suggest that $\tan\beta < 28$ and $g' > 10^{-2}$ [49]. The large upper limit of $\tan\beta$ suggests that $\cos\beta$ should be small, whereas g' is expected to remain sufficiently small to preserve the perturbative nature of the $U(1)$ gauge theory. Furthermore, it is reasonable to assume that $Q_2 - Q_1$ is of $\mathcal{O}(1)$ under the consideration of naturalness. While satisfying these conditions and simultaneously hoping that $T_{Z\gamma}^{WH}$ is as large as possible, we assume that $\cos(\alpha - \beta) \sim \cos\beta \sim \sin\theta_2 \sim \mathcal{O}(10^{-1})$ and $g' \sim (Q_2 - Q_1) \sim \mathcal{O}(1)$. With these assumptions, we can conservatively estimate

$$a \equiv g'(Q_2 - Q_1)\cos(\alpha - \beta)\sin\beta\cos\beta\sin\theta_2 \sim \mathcal{O}(10^{-3}). \quad (30)$$

To make a maximum estimate on $T_{Z\gamma}^{WH}$, let us assume that $|a|$ is close to the margin of $\mathcal{O}(10^{-2})$, *i.e.*, $|a| = 0.01$. With this entry, we plot the magnitude of $T_{Z\gamma}^{WH}$ as a function of m_{H^\pm} in the left panel of Fig. 3. Obviously, $T_{Z\gamma}^{WH}$ decreases as m_{H^\pm} increases: the magnitude of which can only reach $\mathcal{O}(10^{-8})$ GeV $^{-1}$ comparable to that of the b quark loops in the SM (cf. the value of $T_{Z\gamma}^{b,\text{SM}}$ in Eq. (26)), which is one and two orders of magnitude smaller than that of the t quark loops and W loops, respectively. Therefore, the contribution from the W^\pm - H^\pm mixing diagrams is negligible. Below, we merely consider the contributions from the pure charged Higgs diagrams.

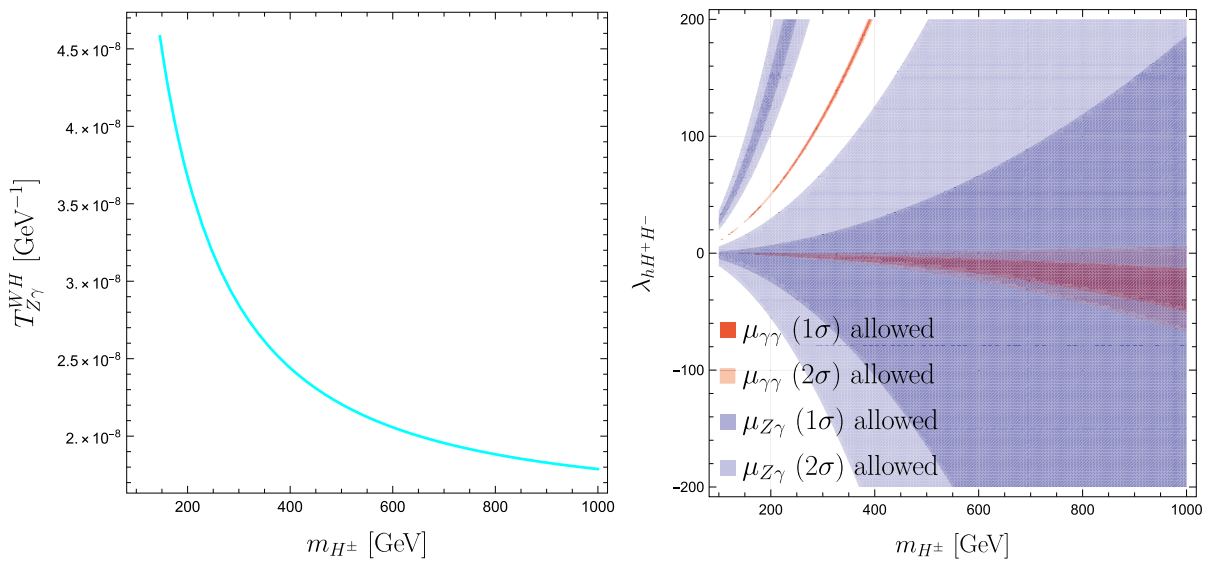


Fig. 3. (color online) Left: Magnitude of $T_{Z\gamma}^{WH}$ as a function of m_{H^\pm} with input $|a| = 0.01$. Right: 1σ and 2σ allowed regions for m_{H^\pm} and $\lambda_{hH^+H^-}$ with constraints from $\mu_{Z\gamma}$ (blue) and $\mu_{\gamma\gamma}$ (red).

In the right panel of Fig. 3, we present the 1σ and 2σ allowed regions for the parameters m_{H^\pm} and $\lambda_{hH^+H^-}$, with constraints derived from $\mu_{Z\gamma}$ (blue) and $\mu_{\gamma\gamma}$ (red). It is clear from this plot that in the parameter regions where $m_{H^\pm} > 200$ GeV and $\lambda_{hH^+H^-} < 0$, both the measured $\mu_{Z\gamma}$ and $\mu_{\gamma\gamma}$ can be accommodated within the 1σ level. Interestingly, the bound on the charged Higgs mass obtained in this work is also consistent with that from the constraints of B observables in Ref. [49] (see the right panel of Fig. 1 in this reference). As discussed above, since $\mu_{\gamma\gamma}$ is better than $\mu_{Z\gamma}$ in terms of the consistency between the SM prediction and measurement, the overlapped parameter regions allowed by the two observables in the right panel of Fig. 3 are mainly narrowed down by the former.

The remaining contribution comes from the fermion loop diagrams, in which FG2HDM influences the $h \rightarrow Z\gamma$ decay by correcting the $f\bar{f}Z$ couplings. As shown in the Feynman diagrams depicted in Figs. 1 and 2, such corrections only influence $\mu_{Z\gamma}$ and leave $\mu_{\gamma\gamma}$ entirely unaffected, as the latter does not involve any $f\bar{f}Z$ vertex. Although the $f\bar{f}Z$ vertex corrections also influence the $h \rightarrow ZZ^*$ decay, as two $f\bar{f}Z$ vertices are involved in such a process, the impact on them is negligible compared with that on the $h \rightarrow Z\gamma$ decay, as the latter contains only one $f\bar{f}Z$ vertex. Therefore, we do not invoke $h \rightarrow ZZ^*$ in the numerical constraints.

Note that the total $f\bar{f}Z$ coupling in Eq. (A5) has been projected into the left-handed part C_L^f and right-handed part C_R^f , with

$$\begin{aligned} C_L^f &= \frac{g_2 \cos\theta_2'}{c_W} (I_f^3 - Q_f s_W^2) + g' \sin\theta_2' Q_{fL}, \\ C_R^f &= -\frac{g_2 \cos\theta_2'}{c_W} Q_f s_W^2 + g' \sin\theta_2' Q_{fR}. \end{aligned} \quad (31)$$

In the limit $\cos\theta_2' \sim 1$ ($\sin\theta_2' \sim 0$), the above expressions restore to the ones in the SM. Given the dominant role of the top quark in contributions from fermion loops, particular emphasis is placed on the correction from the $t\bar{t}Z$ vertex. Using $I_t^3 = 1/2$ and $Q_t = +2/3$ for the top quark, along with the values of s_W and $\alpha(m_Z)$ from Table 2, we obtain $C_L^{t,SM} \simeq 0.256$ and $C_R^{t,SM} \simeq -0.114$. Notice that in Eq. (18) the contribution from the top loops depends on the sum of C_L^t and C_R^t , *i.e.*, the vector coupling $C_V^t \equiv (C_L^t + C_R^t)/2$. Therefore, the deviation $\Delta C_V^t \equiv (\Delta C_L^t + \Delta C_R^t)/2$, where

$$\Delta C_L^t = g' \sin\theta_2' Q_{tL}, \quad \Delta C_R^t = g' \sin\theta_2' Q_{tR}, \quad (32)$$

measures the deviation from the SM, *i.e.*, the contribution from FG2HDM. The measurement of $\mu_{Z\gamma}$ can impose a constraint on ΔC_V^t , which subsequently can be translated into the bounds on the parameters of

FG2HDM.

Besides $\mu_{Z\gamma}$, ΔC_V^t also subjects to constraints from the following two primary sources: i) top quark observables, and ii) the FCNC process $b \rightarrow s\ell^+\ell^-$. Regarding the former, both the CMS [56] and ATLAS [57, 58] collaborations have conducted precise measurements of the differential and/or inclusive cross section of top quark pair production in association with a Z boson at the LHC. ATLAS has also measured the production of single top quark and anti-top quark via the t -channel exchange of a W boson [59]. These measurements align well with their SM predictions and can be leveraged to establish limits on the Wilson coefficients of the SM effective field theory (SMEFT) [60–62]. By invoking the matching between ΔC_V^t and the SMEFT Wilson coefficients [63]:

$$\Delta C_V^t = \frac{g_2 v^2}{2\Lambda^2 c_W} \text{Re} \left[-C_{Hu}^{33} - C_{HQ}^{(1,33)} + C_{HQ}^{(3,33)} \right], \quad (33)$$

where C_{Hu} , $C_{HQ}^{(1)}$, and $C_{HQ}^{(3)}$ denote respectively the Wilson coefficients of the following SMEFT operators,

$$\begin{aligned} O_{Hu} &\equiv (H^\dagger i \overleftrightarrow{D}_\mu H)(\bar{u}\gamma^\mu u), \\ O_{HQ}^{(1)} &\equiv (H^\dagger i \overleftrightarrow{D}_\mu H)(\bar{Q}\gamma^\mu Q), \\ O_{HQ}^{(3)} &\equiv (H^\dagger i \overleftrightarrow{D}_\mu \tau^I H)(\bar{Q}\gamma^\mu \tau^I Q), \end{aligned} \quad (34)$$

we can delineate the permissible range for ΔC_V^t . Adopting the 95% CL intervals provided by ATLAS [58]:

$$C_{Hu}^{33} \in [-2.2, 1.6], \quad C_{HQ}^{(1,33)} \in [-1.4, 0.84], \quad C_{HQ}^{(3,33)} \in [-0.95, 2.0], \quad (35)$$

which are obtained with $\Lambda = 1$ TeV and when one coefficient at a time is assumed to be non-zero, we obtain $\Delta C_V^t \in [-0.076, 0.126]$. Regarding the $b \rightarrow s\ell^+\ell^-$ constraint, the anomalous coupling ΔC_V^t contributes to this FCNC process via the insertion of the $t\bar{t}Z$ vertex into the Z -penguin diagram. This modification affects the Wilson coefficients C_9 and C_{10} , which are associated with the operators $O_9 \equiv (\bar{s}\gamma_\mu P_L b)(\bar{\ell}\gamma^\mu \ell)$ and $O_{10} \equiv (\bar{s}\gamma_\mu P_L b)(\bar{\ell}\gamma^\mu \gamma_5 \ell)$ ($P_L = \frac{1-\gamma_5}{2}$), respectively. Beyond these loop-level effects, FG2HDM introduces additional tree-level FCNC amplitudes that contribute to C_9 and C_{10} . These contributions depend on the same set of model parameters as ΔC_V^t . Consequently, our numerical strategy begins with a comprehensive parameter scan to identify the allowed ranges of the model parameters. These results are then used to determine the viable range for ΔC_V^t . The total corrections to C_9 and C_{10} are expressed as [64]

$$\Delta C_9 = -\frac{1}{N} \left(\frac{1}{m_{Z'}} \mathcal{A}_L^{bsZ'} \mathcal{B}^{Z'\ell\ell} + \frac{1}{m_Z} \mathcal{A}_L^{bsZ} \mathcal{B}^{Z\ell\ell} \right), \quad (36)$$

$$\Delta C_{10} = -\frac{1}{N} \left(\frac{1}{m_{Z'}} \mathcal{A}_L^{bsZ'} \mathcal{B}_5^{Z'\ell\ell} + \frac{1}{m_Z} \mathcal{A}_L^{bsZ} \mathcal{B}_5^{Z\ell\ell} \right), \quad (37)$$

where $N = 2\sqrt{2}G_F V_{tb} V_{ts}^* \alpha / (4\pi)$, and m_Z ($m_{Z'}$) denotes the mass of the Z (Z') boson, representing the contributions from Z -exchange (Z' -exchange) diagrams. The functions \mathcal{A}_L and $\mathcal{B}_{(5)}$ depend on the FG2HDM parameter set $\{g', Q_{\mu R}, Q_{dR}, \sin\theta_2\}$, for which detailed expressions are provided in Ref. [49]. By fixing $\sin\theta_2 = 0.1$, requiring $m_{Z'} < 450$ GeV, and incorporating the established constraints, our scan reveals that ΔC_V^l is constrained within $[-0.05, 0.05]$ at the 3σ level.

Fixing $g' = 1$ and $\sin\theta_2 = 0.1$,¹⁾ and designating Q_{tL} and Q_{tR} as the two independent parameters that need to be restricted, the constraints on which from $\mu_{Z\gamma}$ (blue), top quark observables (orange), and $b \rightarrow s\ell^+\ell^-$ (purple) are shown in Fig. 4. It is clear from this plot that there is an overlapped region for Q_{tL} and Q_{tR} to simultaneously reconcile the three observables. However, due to the relatively large uncertainty, the constraint from $\mu_{Z\gamma}$ is weaker than that from top quark observables and $b \rightarrow s\ell^+\ell^-$. It is also observed that till now the most stringent bound in this respect is taken from the low-energy process $b \rightarrow s\ell^+\ell^-$ decay.

By utilizing the parameters derived above, we evaluate the contributions of different T functions to $\mu_{Z\gamma}$ and $\mu_{\gamma\gamma}$. The results show that $T_{Z\gamma}^W$ and $T_{\gamma\gamma}^W$ are of the order 10^{-5} GeV $^{-1}$, consistent with the SM, whereas $T_{Z\gamma}^H$, $T_{\gamma\gamma}^H$, and $T_{Z\gamma}^l$ are around 10^{-6} GeV $^{-1}$. Due to this clear hierarchy, the W -boson contributions dominate the amplitudes. Interference terms involving W are sub-dominant, and all remaining cross-terms are effectively negligible. This justifies our approach of analysing the constraints from each T function separately rather than accounting for their combined interference effects.

V. CONCLUSION

In this paper, we investigated the $h \rightarrow Z\gamma$ and $h \rightarrow \gamma\gamma$ decays within the framework of FG2HDM. FG2HDM is a BSM model based on the $SU(3)_C \times SU(2)_L \times U(1)_Y \times U(1)'$ gauge symmetry, extending the SM particle spectrum with five additional physical scalars and one neutral gauge boson, Z' . We derived the Feynman rules for the model and calculated the one-loop amplitudes for both decay channels. We found that while both channels are influenced by the charged Higgs bosons, $h \rightarrow Z\gamma$ is uniquely modified by corrections to the $f\bar{f}Z$ vertex. These vertex corrections are also subject to constraints

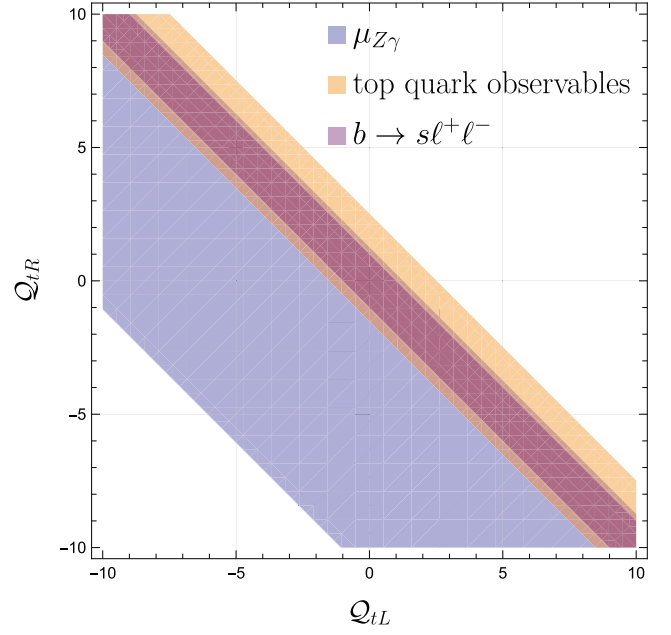


Fig. 4. (color online) The Q_{tL} - Q_{tR} allowed regions obtained from $\mu_{Z\gamma}$ (blue), top quark observables (orange), and $b \rightarrow s\ell^+\ell^-$ (purple), with $g' = 1$ and $\sin\theta_2 = 0.1$.

from top-quark observables and the FCNC process $b \rightarrow s\ell^+\ell^-$. Our numerical analysis demonstrated that the amplitude contributions from W^\pm - H^\pm mixing diagrams are comparable to the SM b -quark loop contributions, which are known to be negligible. Consequently, we focused our analysis on the contributions from pure charged Higgs diagrams. We showed that a parameter region with $m_{H^\pm} > 200$ GeV and $\lambda_{hH^+H^-} < 0$ can simultaneously accommodate both $\mu_{Z\gamma}$ and $\mu_{\gamma\gamma}$ measurements at the 1σ level. This region is primarily constrained by the latter owing to its relatively small uncertainty. Regarding the constraints on the $f\bar{f}Z$ vertex corrections, we considered only the dominant contribution from the top quark. By fixing $g' = 1$ and $\sin\theta_2 = 0.1$, we identified a viable region that simultaneously satisfies the constraints from $\mu_{Z\gamma}$, top-quark observables, and $b \rightarrow s\ell^+\ell^-$, with the strongest constraints coming from $b \rightarrow s\ell^+\ell^-$. In summary, owing to the currently large uncertainty associated with $\mu_{Z\gamma}$, its constraining power is limited compared to other precision observables. Nevertheless, as discussed in the previous section, the HL-LHC with a projected integrated luminosity of 3 ab^{-1} is expected to reduce the relative uncertainty of $\mu_{Z\gamma}$ to 14% [65]. This improvement would significantly strengthen the constraints on FG2HDM.

Note Added. All the authors contribute equally and they are co-first authors, while F. Xu is the corresponding author.

1) The numerical constraints with assigning other values for g' and $\sin\theta_2$ are similar, and they differ from each other only by a rescale factor.

APPENDIX A: LAGRANGIAN AND FEYNMAN RULES

Since at least one photon is involved in both the $h \rightarrow Z\gamma$ and $h \rightarrow \gamma\gamma$ decays, the propagators of the one-loop diagrams shall always be charged particles (see Figs. 1 and 2). Therefore, to calculate the amplitudes we should first identify the Lagrangian that describe the interactions between the charged particles and the Higgs, Z boson, and photon. The formalisms of Feynman rules depend on the choice of gauge. In this paper, we focus on the unitary gauge in which the Goldstone bosons disappear and

only physical particles participate the interactions. After scrutinizing the total Lagrangian provided in Ref. [49], we list the most relevant terms to calculate the amplitudes of $h \rightarrow Z\gamma$ and $h \rightarrow \gamma\gamma$ decays as follows:

$$\mathcal{L}_S = -\lambda_{hH^+H^-} v h H^+ H^-, \quad (\text{A1})$$

$$\mathcal{L}_{SF} = -\frac{1}{v} [\sin(\alpha - \beta) M_f - \cos(\alpha - \beta) N_f] h \bar{f} f, \quad (\text{A2})$$

$$\begin{aligned} \mathcal{L}_{SG} = & \frac{g_2^2 v}{2} \sin(\alpha - \beta) h W_\mu^+ W^{-\mu} - i e A_\mu (\partial^\mu H^+ H^- \partial^\mu H^- H^+) + e^2 A_\mu A^\mu H^+ H^- - i \left[\left(\frac{g_2^2}{2} c_W - \frac{g_1}{2} s_W \right) \cos \theta_2' \right. \\ & + (\sin^2 \beta Q_1 + \cos^2 \beta Q_2) g' \sin \theta_2' \left. \right] Z_\mu (\partial^\mu H^+ H^- \partial^\mu H^- H^+) - i \frac{g_2^2}{2} \cos(\alpha - \beta) \left[\partial^\mu h (W_\mu^+ H^- W_\mu^- H^+) \right. \\ & + h (\partial^\mu H^+ W_\mu^- \partial^\mu H^- W_\mu^+) \left. \right] + g_2 g' (Q_2 - Q_1) v \sin \beta \cos \beta \sin \theta_2' Z^\mu (W_\mu^+ H^- + W_\mu^- H^+) \\ & + 2 g_2 s_W \left[\left(\frac{g_2^2}{2} c_W - \frac{g_1}{2} s_W \right) \cos \theta_2' + (\sin^2 \beta Q_1 + \cos^2 \beta Q_2) g' \sin \theta_2' \right] A_\mu Z^\mu H^+ H^- \\ & - \frac{g_2^2}{2} s_W \cos(\alpha - \beta) A^\mu (H^+ W_\mu^- + H^- W_\mu^+) h, \end{aligned} \quad (\text{A3})$$

$$\begin{aligned} \mathcal{L}_G = & i g_2 c_W \cos \theta_2' \left[(\partial_\mu W_\nu^+ W^{-\mu} Z^\nu - \partial_\mu W_\nu^+ W^{-\nu} Z^\mu) - (\partial_\mu W_\nu^- W^{+\mu} Z^\nu - \partial_\mu W_\nu^- W^{+\nu} Z^\mu) + (\partial_\mu Z_\nu W^{+\mu} W^{-\nu} - \partial_\mu Z_\nu W^{-\mu} W^{+\nu}) \right] \\ & + i g_2 s_W \left[(\partial_\mu W_\nu^+ W^{-\mu} A^\nu - \partial_\mu W_\nu^+ W^{-\nu} A^\mu) - (\partial_\mu W_\nu^- W^{+\mu} A^\nu - \partial_\mu W_\nu^- W^{+\nu} A^\mu) + (\partial_\mu A_\nu W^{+\mu} W^{-\nu} - \partial_\mu A_\nu W^{-\mu} W^{+\nu}) \right] \\ & - g_2^2 s_W c_W \cos \theta_2' \left[2 W_\mu^+ W^{-\mu} A^\nu Z_\nu - W_\mu^+ W^{-\nu} A_\nu Z^\mu - W_\nu^- W^{+\mu} A_\mu Z^\nu \right] - g_2^2 s_W^2 (W_\mu^+ W^{-\mu} A^\nu A_\nu - W_\mu^+ W^{-\nu} A_\nu A^\mu), \end{aligned} \quad (\text{A4})$$

$$\mathcal{L}_{FG} = \frac{g_2 \cos \theta_2'}{c_W} Z_\mu \bar{f} \left[(I_f^3 - Q_f s_W^2) \gamma^\mu P_L - Q_f s_W^2 \gamma^\mu P_R \right] f + g' \sin \theta_2' Z_\mu \bar{f} \left[Q_{fL} \gamma^\mu P_L + Q_{fR} \gamma^\mu P_R \right] f + e Q_f A_\mu \bar{f} \gamma^\mu f. \quad (\text{A5})$$

The first Lagrangian \mathcal{L}_S , which describes the interaction between the neutral and charged Higgs, is obtained by expressing the scalar potential (cf. Eq. (5)) in terms of physical fields and their coupling reads

$$\begin{aligned} \lambda_{hH^+H^-} = & \frac{1}{v} \left[\lambda_1 v_1 \sin \alpha \sin^2 \beta - \lambda_2 v_2 \cos \alpha \cos^2 \beta \right. \\ & + v_1 \cos \beta (\lambda_3 \sin \alpha \cos \beta + \lambda_4 \cos \alpha \sin \beta) \\ & \left. - v_2 \sin \beta (\lambda_3 \cos \alpha \sin \beta + \lambda_4 \sin \alpha \cos \beta) \right]. \end{aligned} \quad (\text{A6})$$

The second Lagrangian \mathcal{L}_{SF} is the Yukawa interactions, with M_f ($f = u, d, \ell$) being the diagonal mass matrices: $M_u = \text{diag}(m_u, m_c, m_t)$, $M_d = (m_d, m_s, m_b)$, and $M_\ell = (e, \mu, \tau)$. Here, M_f is diagonalized by a biunitary transformation:

$$M_f = \frac{1}{\sqrt{2}} U_{fL}^\dagger (v_1 Y_1^f + v_2 Y_2^f) U_{fR}, \quad (\text{A7})$$

where Y_1^f and Y_2^f are Yukawa matrices, and U_{fL} and U_{fR} are unitary matrices. For convenience, we have also introduced the auxiliary matrices N_f , which are defined as

$$N_f = \frac{1}{\sqrt{2}} U_{fL}^\dagger (v_1 Y_2^f - v_2 Y_1^f) U_{fR}. \quad (\text{A8})$$

To investigate the B -anomalies reported in Ref. [49], we employ specific $U(1)'$ charge assignments for the fields. This configuration ensures that tree-level FCNCs emerge specifically in the down-type quark sector. With such assignments, the Yukawa matrices have the following textures:

$$\begin{aligned}
Y_1^u &= \begin{pmatrix} * & * & 0 \\ * & * & 0 \\ 0 & 0 & 0 \end{pmatrix}, & Y_2^u &= \begin{pmatrix} 0 & 0 & 0 \\ 0 & 0 & 0 \\ 0 & 0 & * \end{pmatrix}, \\
Y_1^d &= \begin{pmatrix} * & * & * \\ * & * & * \\ 0 & 0 & 0 \end{pmatrix}, & Y_2^d &= \begin{pmatrix} 0 & 0 & 0 \\ 0 & 0 & 0 \\ * & * & * \end{pmatrix}, \\
Y_1^\ell &= \begin{pmatrix} 0 & 0 & 0 \\ 0 & * & 0 \\ 0 & 0 & * \end{pmatrix}, & Y_2^\ell &= \begin{pmatrix} * & 0 & 0 \\ 0 & 0 & 0 \\ 0 & 0 & 0 \end{pmatrix}, \quad (A9)
\end{aligned}$$

where '*' denotes an arbitrary non-zero number. Then, the auxiliary matrices N_f have the following explicit forms:

$$\begin{aligned}
N_u &= -\frac{v_2}{v_1} \text{diag}(m_u, m_c, 0) + \frac{v_1}{v_2} \text{diag}(0, 0, m_t), \\
(N_d)_{ij} &= -\frac{v_2}{v_1} (M_d)_{ij} + \left(\frac{v_2}{v_1} + \frac{v_1}{v_2}\right) (V_{\text{CKM}}^\dagger)_{i3} (V_{\text{CKM}})_{3j} (M_d)_{jj}, \\
N_\ell &= -\frac{v_2}{v_1} \text{diag}(0, m_\mu, m_\tau) + \frac{v_1}{v_2} \text{diag}(m_e, 0, 0), \quad (A10)
\end{aligned}$$

where V_{CKM} denotes the Cabibbo-Kobayashi-Maskawa (CKM) matrix [10, 11]. The third Lagrangian \mathcal{L}_{SG} describes the interactions between the scalars and the gauge bosons, which is obtained by expanding the scalar kinetic terms with gauge bosons contained in the covariant derivatives. The quantities Q_1 and Q_2 denote respectively the $U(1)'$ charges of Φ_1 and Φ_2 , and s_W and c_W are separately short for $\sin\theta_W$ and $\cos\theta_W$. The fourth Lagrangian \mathcal{L}_G describes the interactions between the gauge bosons, which results from the vector field strength terms. The last Lagrangian \mathcal{L}_{FG} contains the interactions between the fermions and Z boson and photon, where I_f^3 denotes the third component of the weak isospin of a fermion doublet, Q_f denotes the electric charge of a given fermion f , and Q_{fL} and Q_{fR} represent the $U(1)'$ charge of a left-handed and right-handed fermion, respectively. It is also clear from Eq. (A5) that the $Z-Z'$ mixing yields an additional term that has the same Lorentz structure as the SM one, which therefore provides a correction to the original couplings. For more details on FG2HDM Lagrangian in different sectors, refer to Ref. [49].

With the Lagrangian listed in Eqs. (A1)–(A5) at hand, obtaining the Feynman rules for the vertices is straightforward. Besides, the Feynman rules for the propagators of the charged Higgs, W boson, and fermions can be derived directly from the free Lagrangian that we do not show. Working in the unitary gauge, we summarize all the relevant vertices as well as propagators of FG2HDM that are necessary to calculate the amplitudes of the $h \rightarrow Z\gamma$ and $h \rightarrow \gamma\gamma$ decays in Fig. A1.

APPENDIX B: SCALAR FUNCTIONS

In this appendix, we show the analytical expressions for the scalar functions appearing in Sec. III.A and III.B.

$$\begin{aligned}
\Lambda(m_a^2; m_b, m_c) &= \frac{1}{m_a^2} \lambda^{\frac{1}{2}}(m_a^2, m_b^2, m_c^2) \text{Log} \\
&\times \left(\frac{\lambda^{\frac{1}{2}}(m_a^2, m_b^2, m_c^2) - m_a^2 + m_b^2 + m_c^2}{2m_b m_c} \right), \quad (B1)
\end{aligned}$$

$$\begin{aligned}
C_0(m_Z^2, 0, m_h^2, m_i^2, m_i^2, m_i^2) &= \frac{1}{2(m_h^2 - m_Z^2)} \\
&\times \left[\text{Log}^2 \left(\frac{\sqrt{-m_h^2(4m_i^2 - m_h^2)} + 2m_i^2 - m_h^2}{2m_i^2} \right) \right. \\
&\left. - \text{Log}^2 \left(\frac{\sqrt{-m_Z^2(4m_i^2 - m_Z^2)} + 2m_i^2 - m_Z^2}{2m_i^2} \right) \right], \quad (B2)
\end{aligned}$$

$$\begin{aligned}
C_0(0, 0, m_h^2, m_i^2, m_i^2, m_i^2) &= \frac{1}{2m_h^2} \text{Log}^2 \left(\frac{\sqrt{-m_h^2(4m_i^2 - m_h^2)} + 2m_i^2 - m_h^2}{2m_i^2} \right), \quad (B3)
\end{aligned}$$

$$\begin{aligned}
C_0(0, m_h^2, m_Z^2, m_i^2, m_i^2, m_j^2) &= \frac{1}{m_h^2 - m_Z^2} \\
&\times \left\{ -\text{DiLog} \left[\frac{2(m_h^2 + \Delta_{ij})}{m_h^2 + \Delta_{ij} - \lambda^{\frac{1}{2}}(m_h^2, m_i^2, m_j^2)}, m_h^2 + \Delta_{ij} \right] \right. \\
&- \text{DiLog} \left[\frac{2(m_h^2 + \Delta_{ij})}{m_h^2 + \Delta_{ij} + \lambda^{\frac{1}{2}}(m_h^2, m_i^2, m_j^2)}, -(m_h^2 + \Delta_{ij}) \right] \\
&+ \text{DiLog} \left[\frac{2\Delta_{ij}}{m_h^2 + \Delta_{ij} - \lambda^{\frac{1}{2}}(m_h^2, m_i^2, m_j^2)}, \Delta_{ij} \right] \\
&+ \text{DiLog} \left[\frac{2\Delta_{ij}}{m_h^2 + \Delta_{ij} + \lambda^{\frac{1}{2}}(m_h^2, m_i^2, m_j^2)}, -\Delta_{ij} \right] \\
&\left. - (m_h \rightarrow m_Z) \right\}, \quad (B4)
\end{aligned}$$

where $\Delta_{ij} = m_i^2 - m_j^2$, $\lambda(a, b, c) = a^2 + b^2 + c^2 - 2ab - 2ac - 2bc$ is the usual Källén function, and $\text{DiLog}[a, b]$ is a function defined in *Package-X* [54].

APPENDIX C: KINEMATICS

Both $h(p) \rightarrow Z(p_1)\gamma(p_2)$ and $h(p) \rightarrow \gamma(p_1)\gamma(p_2)$ are processes of two-body decays, and its differential decay

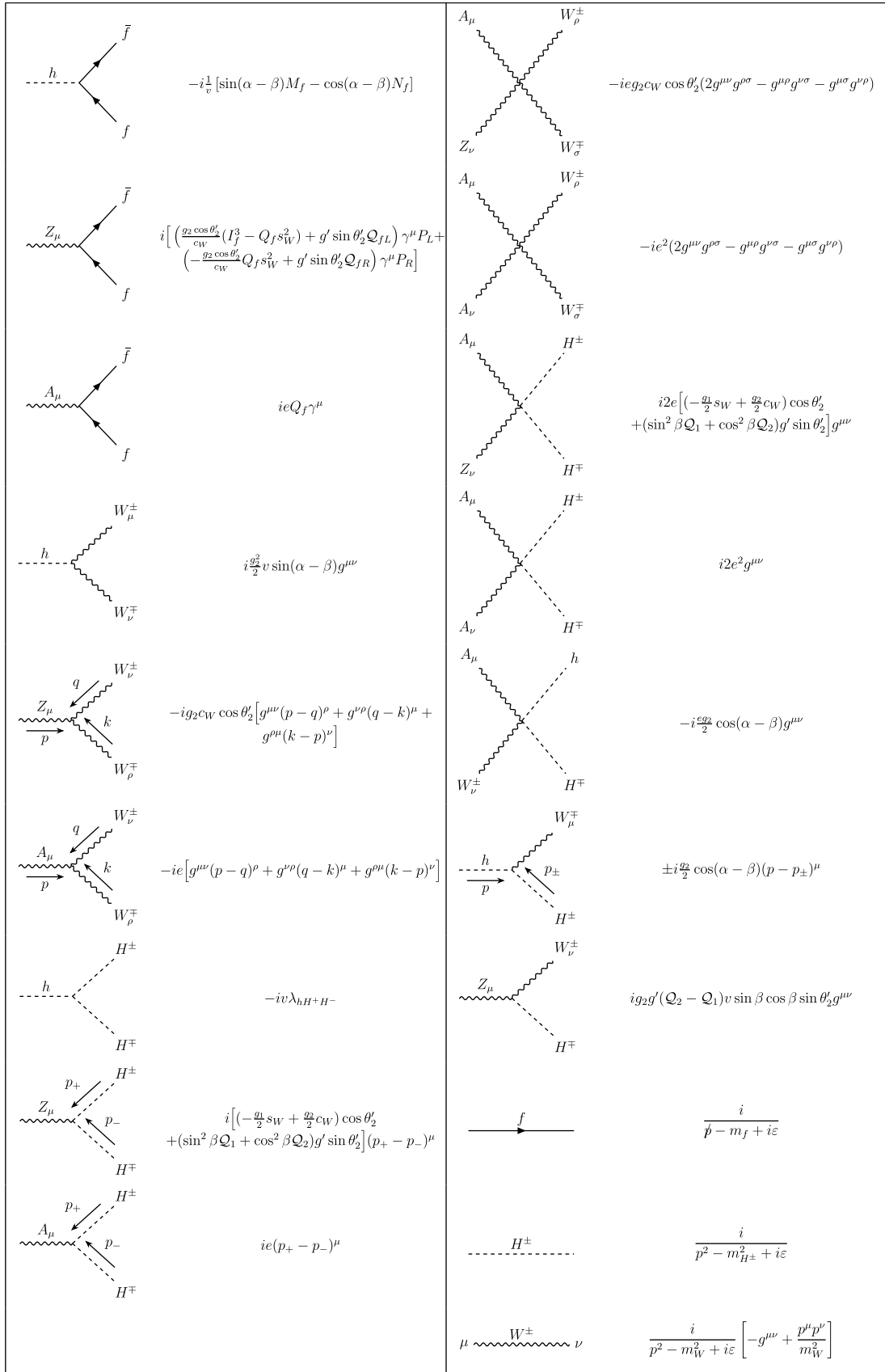


Fig. A1. Feynman rules for the relevant vertices and propagators in the unitary gauge.

width is given by

$$d\Gamma = \frac{1}{2m_h} |\mathcal{M}_X|^2 d\Phi_2, \quad (C1)$$

where \mathcal{M}_X denotes the amplitude, and $d\Phi_2$ is the two-body decay phase space given by

$$d\Phi_2 = \frac{|\vec{p}_1|}{16\pi^2 m_h} d\Omega. \quad (C2)$$

Here, $|\vec{p}_1| = \lambda^{1/2}(m_h^2, m_1^2, m_2^2)/2m_h$, which is equal to $(m_h^2 - m_2^2)/2m_h$ for $h \rightarrow Z\gamma$ and $m_h/2$ for $h \rightarrow \gamma\gamma$, respectively; $d\Omega = d\phi_1 d\cos\theta_1$ is the solid angle of particle 1 in the final state, which, after integration, yields 4π . To calculate the decay width or branching ratio of the two processes, one has to sum over the spins of the Z boson and photon in the final state:

$$\begin{aligned} \sum_{\lambda_1, \lambda_2} |\mathcal{M}_X|^2 &= |T_X|^2 (p_2^\mu p_1^\nu - p_1 \cdot p_2 g^{\mu\nu}) (p_2^\alpha p_1^\beta - p_1 \cdot p_2 g^{\alpha\beta}) \\ &\times \sum_{\lambda_1, \lambda_2} [\epsilon_\mu^*(p_1, \lambda_1) \epsilon_\alpha(p_1, \lambda_1)] [\epsilon_\nu^*(p_2, \lambda_2) \epsilon_\beta(p_2, \lambda_2)]. \end{aligned} \quad (C3)$$

For $X = Z\gamma$, one has

$$\begin{aligned} &\sum_{\lambda_1, \lambda_2} [\epsilon_\mu^*(p_1, \lambda_1) \epsilon_\alpha(p_1, \lambda_1)] [\epsilon_\nu^*(p_2, \lambda_2) \epsilon_\beta(p_2, \lambda_2)] \\ &= \left(-g_{\mu\alpha} + \frac{p_{1\mu} p_{1\alpha}}{m_Z^2} \right) (-g_{\nu\beta}). \end{aligned} \quad (C4)$$

Substituting this into Eqs. (C3) and (C1) and dividing by the total Higgs decay width Γ_h yields the branching fraction for $h \rightarrow Z\gamma$,

$$\mathcal{B}(h \rightarrow Z\gamma) = \frac{m_h^3}{32\pi\Gamma_h} \left(1 - \frac{m_Z^2}{m_h^2} \right)^3 |T_{Z\gamma}|^2. \quad (C5)$$

Similarly, for $X = \gamma\gamma$, one has

$$\sum_{\lambda_1, \lambda_2} [\epsilon_\mu^*(p_1, \lambda_1) \epsilon_\alpha(p_1, \lambda_1)] [\epsilon_\nu^*(p_2, \lambda_2) \epsilon_\beta(p_2, \lambda_2)] = (-g_{\mu\alpha}) (-g_{\nu\beta}), \quad (C6)$$

and the branching fraction for $h \rightarrow \gamma\gamma$ reads

$$\mathcal{B}(h \rightarrow \gamma\gamma) = \frac{m_h^3}{64\pi\Gamma_h} |T_{\gamma\gamma}|^2. \quad (C7)$$

In deriving Eq. (C7), since there are two identical photons in the final state, an additional $1/2$ factor is taken into account.

References

- [1] G. Aad *et al.* (ATLAS Collaboration), *Phys. Lett. B* **716**, 1 (2012), arXiv: 1207.7214[hep-ex]
- [2] S. Chatrchyan *et al.* (CMS Collaboration), *Phys. Lett. B* **716**, 30 (2012), arXiv: 1207.7235[hep-ex]
- [3] S. Chatrchyan *et al.* (CMS Collaboration), *JHEP* **06**, 081 (2013), arXiv: 1303.4571[hep-ex]
- [4] T. D. Lee, *Phys. Rev. D* **8**, 1226 (1973)
- [5] S. L. Glashow and S. Weinberg, *Phys. Rev. D* **15**, 1958 (1977)
- [6] E. A. Paschos, *Phys. Rev. D* **15**, 1966 (1977)
- [7] A. Pich and P. Tuzon, *Phys. Rev. D* **80**, 091702 (2009), arXiv: 0908.1554[hep-ph]
- [8] M. Jung, A. Pich, and P. Tuzon, *JHEP* **11**, 003 (2010), arXiv: 1006.0470[hep-ph]
- [9] P. M. Ferreira, L. Lavoura, and J. P. Silva, *Phys. Lett. B* **688**, 341 (2010), arXiv: 1001.2561[hep-ph]
- [10] N. Cabibbo, *Phys. Rev. Lett.* **10**, 531 (1963)
- [11] M. Kobayashi and T. Maskawa, *Prog. Theor. Phys.* **49**, 652 (1973)
- [12] G. C. Branco, W. Grimus, and L. Lavoura, *Phys. Lett. B* **380**, 119 (1996), arXiv: hep-ph/9601383
- [13] A. Celis, J. Fuentes-Martin, M. Jung *et al.*, *Phys. Rev. D* **92**, 015007 (2015), arXiv: 1505.03079[hep-ph]
- [14] A. Ordell, R. Pasechnik, H. Serôdio *et al.*, *Phys. Rev. D* **100**, 115038 (2019), arXiv: 1909.05548[hep-ph]
- [15] A. Ordell, R. Pasechnik, and H. Serôdio, *Phys. Rev. D* **102**, 035016 (2020), arXiv: 2006.08676[hep-ph]
- [16] P. M. Ferreira, F. F. Freitas, J. a. Gonçalves *et al.*, *Phys. Rev. D* **106**, 075017 (2022), arXiv: 2202.13153[hep-ph]
- [17] G. Aad *et al.* (ATLAS Collaboration), *Phys. Lett. B* **809**, 135754 (2020), arXiv: 2005.05382[hep-ex]
- [18] A. Tumasyan *et al.* (CMS Collaboration), *JHEP* **05**, 233 (2023), arXiv: 2204.12945[hep-ex]
- [19] G. Aad *et al.* (ATLAS and CMS Collaborations), *Phys. Rev. Lett.* **132**, 021803 (2024a), arXiv: 2309.03501[hep-ex]
- [20] A. Khodjamirian, K. Melnikov, and A. Vainshtein, (2025), arXiv: 2512.02165[hep-ph]
- [21] M. Spira, A. Djouadi, and P. M. Zerwas, *Phys. Lett. B* **276**, 350 (1992)
- [22] T. Gehrmann, S. Guns, and D. Kara, *JHEP* **09**, 038 (2015), arXiv: 1505.00561[hep-ph]
- [23] R. Bonciani, V. Del Duca, H. Frellesvig *et al.*, *JHEP* **08**, 108 (2015), arXiv: 1505.00567[hep-ph]
- [24] F. Buccioni, F. Devoto, A. Djouadi *et al.*, *Phys. Lett. B* **851**, 138596 (2024), arXiv: 2312.12384[hep-ph]
- [25] Z. Q. Chen, L. B. Chen, C. F. Qiao *et al.*, *Phys. Rev. D* **110**, L051301 (2024), arXiv: 2404.11441[hep-ph]
- [26] W. L. Sang, F. Feng, and Y. Jia, *Phys. Rev. D* **110**, L051302 (2024), arXiv: 2405.03464[hep-ph]
- [27] S. Panghal and B. Mukhopadhyaya, (2023), arXiv: 2310.04136[hep-ph]
- [28] G. Lichtenstein, M. A. Schmidt, G. Valencia *et al.*, *Nucl. Phys. B* **1013**, 116850 (2025), arXiv: 2312.09409[hep-ph]
- [29] T. T. Hong, V. K. Le, L. T. T. Phuong *et al.*, *PTEP* **2024**, 033B04 (2024) [Erratum: *PTEP* **2024**, 059201 (2024)], arXiv: 2312.11045[hep-ph]

- [30] R. Boto, D. Das, J. C. Romao *et al.*, *Phys. Rev. D* **109**, 095002 (2024a), arXiv: 2312.13050[hep-ph]
- [31] N. Das, T. Jha, and D. Nanda, *Phys. Rev. D* **109**, 115020 (2024), arXiv: 2402.01317[hep-ph]
- [32] K. Cheung and C. J. Ouseph, *Phys. Rev. D* **110**, 055016 (2024), arXiv: 2402.05678[hep-ph]
- [33] X. G. He, Z. L. Huang, M. W. Li *et al.*, *JHEP* **10**, 135 (2024), arXiv: 2402.08190[hep-ph]
- [34] B. A. Ouazghour, M. Chabab, and K. Goure, *Eur. Phys. J. C* **84**, 879 (2024), arXiv: 2403.07722[hep-ph]
- [35] A. Arhrib, K. H. Phan, V. Q. Tran *et al.*, (2024), arXiv: 2405.03127[hep-ph]
- [36] A. I. Hernández-Juárez, R. Gaitán, and R. Martínez, *Phys. Rev. D* **111**, 015001 (2025), arXiv: 2405.03094[hep-ph]
- [37] C. Grojean, G. Guedes, J. Roosmale Nepveu *et al.*, *JHEP* **12**, 065 (2024), arXiv: 2405.20371[hep-ph]
- [38] H. c. Hu, Z. Y. Zhang, N. Y. Zhu *et al.*, *Chin. Phys. C* **48**, 093101 (2024), arXiv: 2406.00946[hep-ph]
- [39] A. Arhrib, R. Benbrik, L. Rahili *et al.*, *Eur. Phys. J. C* **84**, 799 (2024b), arXiv: 2406.13001[hep-ph]
- [40] K. H. Phan, D. T. Tran, and T. H. Nguyen, *PTEP* **2025**, 023B05 (2025), arXiv: 2406.15749[hep-ph]
- [41] S. Israr and M. Rehman, *Eur. Phys. J. Plus* **140**, 397 (2025), arXiv: 2407.01210[hep-ph]
- [42] K. Mantzaropoulos, *Phys. Rev. D* **110**, 055041 (2024), arXiv: 2407.09145[hep-ph]
- [43] R. Boto, P. N. Figueiredo, J. C. Romão *et al.*, *JHEP* **11**, 108 (2024), arXiv: 2407.15933[hep-ph]
- [44] D. Barducci, L. Di Luzio, M. Nardecchia *et al.*, *JHEP* **12**, 154 (2023), arXiv: 2311.10130[hep-ph]
- [45] ATLAS Collaboration (ATLAS Collaboration), ATLAS-CONF-2025-007 (2025)
- [46] J. F. Gunion, H. E. Haber, G. L. Kane *et al.*, *The Higgs Hunter's Guide*, Vol. 80 (2000)
- [47] A. Djouadi, *Phys. Rept.* **457**, 1 (2008), arXiv: hep-ph/0503172
- [48] S. Navas *et al.* (Particle Data Group), *Phys. Rev. D* **110**, 030001 (2024)
- [49] Q. Wen and F. Xu, *Phys. Rev. D* **111**, 115024 (2025)
- [50] D. Fontes, J. C. Romão, and J. a. P. Silva, *JHEP* **12**, 043 (2014), arXiv: 1408.2534[hep-ph]
- [51] G. Aad *et al.* (ATLAS Collaboration), *Phys. Lett. B* **732**, 8 (2014), arXiv: 1402.3051[hep-ex]
- [52] S. Chatrchyan *et al.* (CMS Collaboration), *Phys. Lett. B* **726**, 587 (2013b), arXiv: 1307.5515[hep-ex]
- [53] L. Bergstrom and G. Hulth, *Nucl. Phys. B* **259**, 137 (1985) [Erratum: *Nucl. Phys. B* **276**, 744 (1986)]
- [54] H. H. Patel, *Comput. Phys. Commun.* **197**, 276 (2015), arXiv: 1503.01469[hep-ph]
- [55] D. de Florian *et al.* (LHC Higgs Cross Section Working Group), **2/2017** (2016), 10.23731/CYRM-2017-002, arXiv: 1610.07922[hep-ph]
- [56] A. M. Sirunyan *et al.* (CMS Collaboration), *JHEP* **03**, 056 (2020), arXiv: 1907.11270[hep-ex]
- [57] G. Aad *et al.* (ATLAS Collaboration), *Eur. Phys. J. C* **81**, 737 (2021), arXiv: 2103.12603[hep-ex]
- [58] G. Aad *et al.* (ATLAS Collaboration), *JHEP* **07**, 163 (2024), arXiv: 2312.04450[hep-ex]
- [59] G. Aad *et al.* (ATLAS Collaboration), *JHEP* **05**, 305 (2024), arXiv: 2403.02126[hep-ex]
- [60] W. Buchmuller and D. Wyler, *Nucl. Phys. B* **268**, 621 (1986)
- [61] B. Grzadkowski, M. Iskrzynski, M. Misiak *et al.*, *JHEP* **10**, 085 (2010), arXiv: 1008.4884[hep-ph]
- [62] I. Brivio and M. Trott, *Phys. Rept.* **793**, 1 (2019), arXiv: 1706.08945[hep-ph]
- [63] J. A. Aguilar-Saavedra, *Nucl. Phys. B* **812**, 181 (2009), arXiv: 0811.3842[hep-ph]
- [64] Q. Wen and F. Xu, *Phys. Rev. D* **108**, 095038 (2023), arXiv: 2305.19038[hep-ph]
- [65] G. Aad *et al.* (ATLAS, CMS), (2025), arXiv: 2504.00672[hep-ex]